HCO+ dissociation in a strong laser field: An ab initio classical trajectory study

Suk Kyoung Lee, Wen Li, H. Bernhard Schlegel *

Department of Chemistry, Wayne State University, Detroit, Michigan 48202, USA

ARTICLE INFO

ABSTRACT

We have investigated the photodissociation of HCO+ in a strong field with a wavelength of 10 μm using ab initio molecular dynamics. Classical trajectories were calculated at three field intensities. At 2.9×10^{14} W/cm² and phase $\phi = 0$, protons have two distinct dissociation times, mainly due to the reorientation of HCO+ relative to the field direction prior to dissociation. The kinetic energy distribution at this intensity agrees with Wardlaw's wagging tail model, suggesting that dissociation occurs through barrier-suppression. At 1.7×10^{14} and 8.8×10^{13} W/cm², barrier suppression is incomplete and the maximum kinetic energy is less than predicted by the wagging tail model.

© 2012 Elsevier B.V. All rights reserved.

1. Introduction

The electronic and nuclear response of a molecule in a strong laser field has attracted great attention in recent years due to its many potential applications such as coherent control [1,2], production of attosecond pulses [3,4] and high energy photon sources [5,6]. In particular, efforts to understand strong field dissociation of a molecule have been made experimentally [7–13] and theoretically [14–20]. A dissociation adiabaticity parameter has been proposed to characterize the dynamics of dissociation [21]. Paci et al. modified it for a heteronuclear diatomic system [22]: $\gamma_{mol} \equiv (D_e/2U_p)^{1/2}$ where $U_p = (\mu/m_c)^2 U_{pm}$. D_e is the dissociation energy of the ground state, μ is the reduced mass, m_c is the mass of the charged fragment and U_{pm} is the ponderomotive potential ($U_{pm} = q^2 E_{max}^2/4\mu\omega^2$), where q is the charge, E_{max} is the maximum electric field strength and ω is the laser frequency). They suggested that this adiabaticity parameter can be used to choose the best way to describe the dissociation: either as multiphoton above-threshold dissociation ($\gamma_{mol} > 1$) or barrier-suppressed dissociation ($\gamma_{mol} < 1$). At long wavelengths, it is known that dissociation generally proceeds through the suppression of a barrier by the strong coupling of the charge distribution to the laser field [10], [23]. In this case, the effect of the field on the dissociation dynamics cannot be handled by perturbative methods. The treatment of the classical dynamics on the changing potential energy surface as the field oscillates was referred to as the 'wagging tail' model by Thachuk and Wardlaw [24]. Using this model, they predicted the maximum kinetic energy of dissociation products from diatomics.

$$KE_{max} = 0.25D_e + 2\sqrt{2D_e}\sqrt{U_{pm}} + 8U_{pm} \qquad (1)$$

The modeling of strong field dissociation, especially for polyatomics, can be difficult. Accurate solution of the full time-dependent Schrödinger equation (TDSE) becomes prohibitively expensive for systems larger than H₂. Ab initio molecular dynamics (AIMD) based on the Born–Oppenheimer approximation and classical mechanics is capable of modeling larger systems with good accuracy and has been successfully applied in a few strong field systems. Previously, the velocity Verlet method [25] was used to integrate the trajectories of molecules in strong laser fields [26]. However, the time efficiency of this method is not ideal for investigating the interesting chemistry of more complex systems in strong fields. In this report, we employed a modified Hessian-based predictor–corrector method with Hessian updating to study HCO+ strong field dissociation.

2. Method

Ab initio classical trajectories were computed with the development version of the GAUSSIAN series of programs [27] using the B3LYP density functional with the 6-311G(d,p) basis set. The classical trajectories were calculated on the adiabatic ground state potential energy surface (i.e. field-induced surface hopping [28] was not included). Energies, gradients and Hessians were calculated in a time-dependent uniform electric field using the Coulomb gauge. Since the gradients and Hessians do not depend on the origin used for the electric field, the classical dynamics are independent of the choice of origin. For the relaxed scans to calculate the effect of the electric field on the bond dissociation potential (Figure 3 inset), the field origin was placed at the center of mass.

Classical trajectories were integrated with a Hessian-based predictor–corrector (HPC) method. This involves a predictor step on a local quadratic surface obtained from a Hessian calculation, followed by a corrector step [29]. For the field-free case, the HPC integrator uses a fifth-order polynomial surface for the corrector

* Corresponding author. Fax: +1 313 577 8822.
E-mail address: hbs@chem.wayne.edu (H. Bernhard Schlegel).
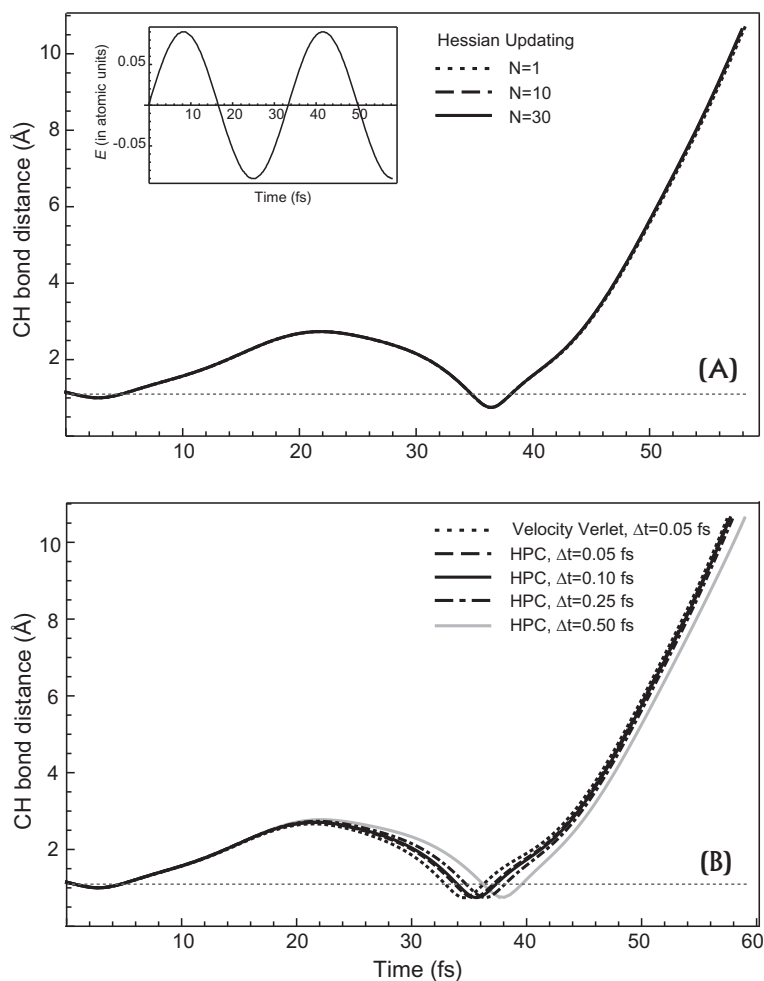
Figure 1. The CH bond distance for a selected trajectory. (A) Effect of Hessian updating with a time step of 0.25 fs (the Hessian was updated for N-1 steps and recalculated at the Nth step). (B) Effect of different time steps for HPC and $N = 10$ compared with velocity Verlet. Trajectories were computed with the laser intensity of 2.9×10^{14} W/cm^2 and the field direction aligned with the molecular axis. The inset shows the time evolution of the laser field. The dotted horizontal gray line represents the equilibrium CH distance.

step. However, for the trajectories in intense fields, the corrector step uses a fourth-order polynomial surface fitted to the energy, gradient and Hessian at the beginning of the predictor step and the gradient and Hessian at the end of the predictor step (HPC-4). An improved Hessian updating scheme for trajectory calculations was recently reported by Hase and coworkers (the change in the Hessian is double of that used for geometry optimization) [30]. This Hessian update was used for N-1 steps before recalculating a new analytical Hessian at the Nth step. To determine appropriate parameters for the HPC-4 integrator, we calculated trajectories of HCO$^+$ in a CW laser field with the same initial conditions and various time steps and numbers of updates. The plot of the CH bond distance vs. time in Figure 1 shows the proton moving away from CO, returning and being driven into the repulsive wall region before dissociating. The time varying electric field ($E(t) = E_{max} \sin(\omega t + \phi)$) is shown in the inset. The details of the dissociation dynamics are discussed below. Each trajectory was simulated for ~60 fs using the HPC-4 integrator and compared with the velocity Verlet method with a time step of 0.05 fs. As seen in Figure 1A, the result with Hessian updating for $N = 30$ is as good as the one with a full Hessian calculation at each step ($N = 1$). In Figure 1B, there is a small variation of the proton returning time depending on the step size. With a time step of 0.5 fs and larger, the shift of the returning time becomes significant. Based on these results, we used the HPC-4 integrator with a step size of 0.25 fs,

updating the Hessian for 9 steps and recalculating the Hessian every 10th step ($N = 10$) to investigate the dissociation dynamics of HCO$^+$ in a strong field. Compared to velocity Verlet, the HPC-4 integrator is ca. five times faster for this small system. For larger systems and longer simulation times, the HPC method could be more efficient.

3. Results and discussion

Ab initio classical trajectories in a CW laser field with an angular frequency of $\omega = 0.188$ radian fs^{-1} (10 μm) were computed at three intensities of 8.8×10^{13}, 1.7×10^{14} and 2.9×10^{14} W/cm^2 (corresponding to maximum field strengths of $E_{max} = 0.05$, 0.07 and 0.09 in atomic units, respectively). A total of 400 trajectories were integrated for up to 0.75 ps for each intensity with phase $\phi = 0$, shown in Figures 2A and 3. An additional 200 trajectories were integrated for 2.9×10^{14} W/cm^2 with phase $\phi = 90°$, shown in Figure 2B. The molecule was placed on the z-axis and the direction of the field for each trajectory was chosen randomly (i.e. uniformly distributed on a sphere). The classical trajectories were started from the equilibrium geometry and were given zero point energy in each normal mode with the vibrational phase chosen randomly; the rotational energy was set to zero. Trajectories were terminated when the distance of the atoms in the two fragments was over 6.35 Å (12 bohr).

(A)

(B)

(C)
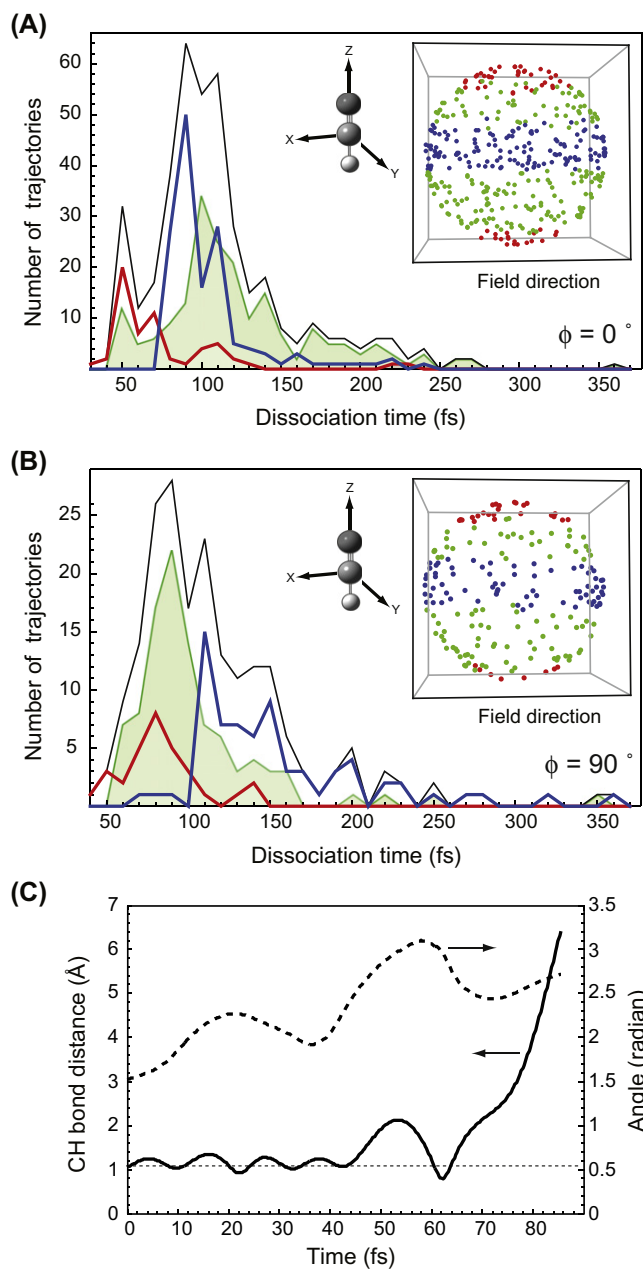
Figure 2. HCO$^+$ dissociation times for $I = 2.9 \times 10^{14}$ W/cm^2 and $\lambda = 10$ μm with (A) phase $\phi = 0°$ and (B) phase $\phi = 90°$. The fragments are considered dissociated when they are 6.35 Å (12 bohr) apart. The electric fields were applied in random orientations with respect to the molecular coordinate system (see insets). Red curves and dots correspond to small angles with respect to the molecular axis (0–40° and 150–180°), green indicates intermediate angles (40–70° and 100–150°) and blue designates nearly perpendicular orientations (70–100°). The uncertainties can be estimated by $N^{1/2}$, where N is the number of trajectories in each bin. (C) The CH bond distance (solid line) and the angle (dashed line) between the field direction and the proton recoil direction of a slow dissociation trajectory. The dotted horizontal gray line represents the equilibrium CH distance. (For interpretation of the references to color in this figure legend, the reader is referred to the web version of this Letter.)

For the selected conditions, the rate of ionization is small compared to dissociation. The calculated ionization potential of HCO$^+$ is ~26.7 eV at the CCSD(T)/6-311++G(2df,2pd) level of theory. Using a modified ADK model [31,32], the estimated ionization rate of HCO$^+$ is about 2.4×10^9 s^{-1} at the highest intensity employed in our study, yielding an ionization probability of ca. 0.0009 for the longest pulse length of laser ($t = 0.37$ ps). Since this probability is small, we have ignored further ionization during dissociation.

The dissociation times of HCO$^+$ in a field with an intensity of 2.9×10^{14} W/cm^2 and phase $\phi = 0$, Figure 2A, show an interesting bimodal distribution with fast (~50 fs) and slow (>80 fs) dissociations. The fast dissociations are complete within ca 2 laser cycles. A typical trace of a proton from a fast dissociation is shown in Figure 1, where the CH bond is stretched to more than twice its equilibrium value in the first half cycle and compressed to less than the equilibrium distance in the next half cycle. The proton has gained considerable kinetic energy during this first full cycle. After reaching the inner turning point, it is accelerated toward dissociation during the next half cycle. The excursion of the proton to large distances followed by recollision with the repulsive wall of the potential is analogous to the electron rescattering dynamics in high harmonic generation and above threshold ionization [33]. This process is sensitive to the wavelength, polarization and phase of laser pulse and is not observed with a shorter wavelength driving laser (e.g. 2 μm). When the frequency of the strong laser field is sufficiently lower than the vibrational frequency of the proton, it can cause large amplitude motion of the proton.

A closer look at the trajectories reveals that the two distinct dissociation times seen in Figure 2A are related to the initial direction and phase of a laser field. Dissociations happen rapidly when the barrier is suppressed as described by the wagging tail model. Examining the trajectories for the highest intensity shows that for fast dissociation, the barrier must be fully suppressed by the time the C–H bond elongates to ca 2 Å. This requires the field to be near its maximum and the C–H bond to be well aligned with the field. When the field is initially oriented along the molecular axis, the field causes little or no rotation of the molecule and dissociation occurs by barrier suppression at one of the early peaks in the field. As a result, the C–H bond reaches dissociation (>12 bohr) in 40–70 fs (shown in red). When the field makes a significant angle with the molecular axis, the field causes the molecule to rotate toward the field direction before dissociating when the barrier is suppressed again. The time required for the rotation depends on the initial angle between the C–H bond and the field. The time needed for a rotation of ca 90° coincides with the timing for the next barrier suppression and accounts for dissociations between 80 and 120 fs (shown in blue). A trajectory with this behavior is illustrated in Figure 2C. For intermediate angles, the distribution of dissociation times is much broader because the rotation times are not necessarily in step with the barrier suppression times (Figure 2 A, shaded in green). Nevertheless peaks occur at ca 40–60 and 90–120 fs resulting from barrier suppression by the field. At times between these peaks, very few trajectories have the required alignment with the field for full barrier suppression followed by dissociation. Changing the initial phase of the vibrational motion but keeping the same set of random orientations of the field yields a similar two peaked distribution (not shown). However, shifting the phase of the field alters the timing of the barrier suppressions and molecular rotations. For a phase of $\phi = 90°$, shown in Figure 2B, the distribution has only one peak. Nevertheless, when the field initially makes small to intermediate angles with the molecular axis (red and green curves), less rotation is required and the dissociations occur more rapidly than when the field is initially perpendicular to the molecular axis (shown in blue). At lower intensities (8.8×10^{13} and 1.7×10^{14} W/cm^2), we cannot detect two distinct dissociation times. In these cases, barrier suppression by the field is not as strong and dissociations occur primarily by the accumulation of vibrational energy.

The alignment between the bond dissociation and the field can be gauged by $\langle \cos^2(\theta) \rangle$, where θ is the angle between the field direction and the final ejection direction of H$^+$. For the results in Figure 2A (phase = 0°), $\langle \cos^2(\theta) \rangle = 0.94$, 0.83 and 0.86 for small, intermediate and perpendicular angles between the field direction and the molecule at the start of the trajectories. The corresponding
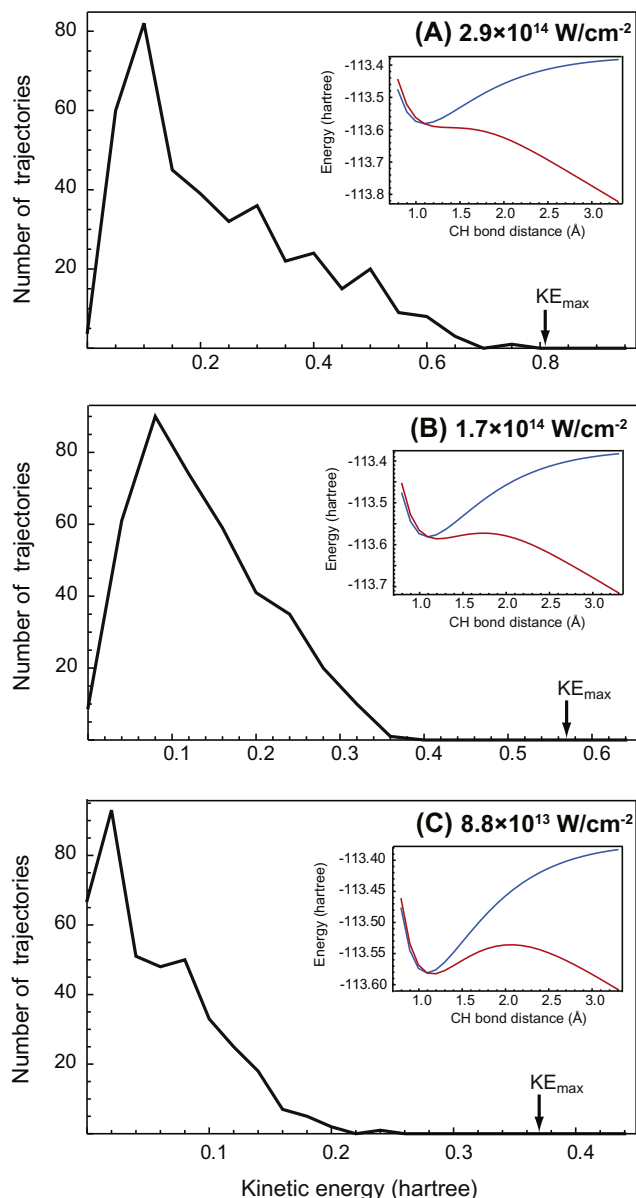
Figure 3. The proton kinetic energy distribution of HCO$^+$ dissociation at the intensities of (A) 2.9×10^{14}, (B) 1.7×10^{14} and (C) 8.8×10^{13} W/cm^2 and phase $\phi = 0°$. The arrows shown in each plot indicate the maximum kinetic energies calculated using the wagging tail model [24]. The uncertainties can be estimated by $N^{1/2}$, where N is the number of trajectories in each bin. The insets show the CH dissociation potentials with and without a static field for each field strength.

values for Figure 2B (phase = 90°) are $\langle \cos^2(\theta) \rangle$ = 0.90, 0.90 and 0.84, respectively. This indicates that the protons are ejected primarily along the field direction. The preferential deflection of fragments along the laser polarization direction was detected experimentally for the multi-photon dissociative ionization of iodine [34]. This extremely high degree of anisotropy reflects the high nonlinearity of the dissociation process.

The dissociation adiabaticity parameter, γ_{mol}, has been used to characterize strong field dissociations. The calculated parameters for HCO$^+$ are 2.7, 1.9 and 1.5 at 8.8×10^{13}, 1.7×10^{14} and 2.9×10^{14} W/cm^2, respectively. These values are at the boundary between the two dissociation regimes, multiphoton above-threshold dissociation for $\gamma_{mol} > 1$ and barrier-suppressed dissociation for $\gamma_{mol} < 1$. Further details of the dissociation dynamics can be obtained by examining the kinetic energy distribution of the ejected proton, shown in Figure 3 for phase $\phi = 0°$. The velocity at the end

of the trajectory was corrected for the quiver motion of a free proton $v_{quiver}(t) = (E_{max}/\mu\omega)\cos(\omega t)$ in the electric field $E(t) = E_{max}\sin(\omega t)$, where t is the time the trajectory is terminated. This yields a corrected kinetic energy, $KE = \frac{1}{2}m(v - v_{quiver})^2$. The kinetic energy distributions of the fast and slow dissociations at the highest intensity are similar. The kinetic energy distribution for $I = 2.9 \times 10^{14}$ W/cm^2 is in good agreement with the maximum kinetic energy predicted by the wagging tail model, Eq. (1). For phase $\phi = 90°$, the distribution is peaked at lower energies but still extends to the maximum kinetic energy predicted by the wagging tail model (not shown). The inset in Figure 3A shows that the dissociation barrier is completely suppresses for $I = 2.9 \times 10^{14}$ W/cm^2, in keeping with a small value of the adiabaticity parameter. For lower intensities, the maximum kinetic energy is less than expected by the wagging tail model. One reason may be the simplifying assumptions used to obtain the wagging tail model. Eq. (1) was based on fitting to the results of classical trajectories calculated with a Morse potential and a linear interaction with the field [24]. The present work uses electronic structure calculations to determine the energy of the molecule in the field, yielding a dipole moment that depends nonlinearly on the bond length and the applied field. Additional factors that contribute to the difference include energy flowing into other degrees of freedom (e.g. HCO bend and CO stretch) and incomplete suppression of the barrier at lower intensities.

4. Conclusion

We have studied HCO$^+$ dissociation in a strong field using ab initio classical trajectory calculations with a modified Hessian-based integrator. The HPC-4 method exhibits fivefold better efficiency than the velocity Verlet method with the same accuracy. With a CW laser at 10 μm and a field intensity of 2.9×10^{14} W/cm^2, some of the protons are ejected within 50 fs in the direction of the field. For the dissociation processes taking place near 100 fs, the initial field is approximately perpendicular to the molecular axis and the molecule must rotate toward the field direction before dissociating. For the photodissociation of HCO$^+$ at the highest intensity, the kinetic energy distribution of the ejected H$^+$ agrees well with the prediction of the wagging tail model. For lower intensities, the adiabaticity parameter is larger, the barrier suppression is incomplete and the maximum kinetic energy is not as large as predicted by the wagging tail model.

Acknowledgements

References

[1] R.J. Levis, G.M. Menkir, H. Rabitz, Science 292 (2001) 709.
[2] A. Assion et al., Science 282 (1998) 919.
[3] J. Zhou, J. Peatross, M.M. Murnane, H.C. Kapteyn, I.P. Christov, Phys. Rev. Lett. 76 (1996) 752.
[4] M. Hentschel et al., Nature 414 (2001) 509.
[5] Z. Chang, A. Rundquist, H. Wang, M.M. Murnane, H.C. Kapteyn, Phys. Rev. Lett. 79 (1997) 2967.
[6] M.C. Chen et al., Phys. Rev. Lett. 105 (2010) 173901.
[7] J.H. Posthumus, Rep. Prog. Phys. 67 (2004) 623.
[8] A.S. Alnaser et al., J. Phys. B 39 (2006) S485.
[9] T. Okino et al., Chem. Phys. Lett. 423 (2006) 220.
[10] P. Dietrich, P.B. Corkum, J. Chem. Phys. 97 (1992) 3187.
[11] A. Zavriyev, P.H. Bucksbaum, H.G. Muller, D.W. Schumacher, Phys. Rev. A 42 (1990) 5500.
[12] R.J. Levis, M.J. DeWitt, J. Phys. Chem. A 103 (1999) 6493.
[13] A.N. Markevitch, S.M. Smith, D.A. Romanov, H.B. Schlegel, M.Y. Ivanov, R.J. Levis, Phys. Rev. A 68 (2003) 013401.

[14] M. Uhlmann, T. Kunert, F. Grossmann, R. Schmidt, Phys. Rev. A 67 (2003) 013413.
[15] M. Thachuk, M.Y. Ivanov, D.M. Wardlaw, J. Chem. Phys. 105 (1996) 4094.
[16] H. Kono, Y. Sato, N. Tanaka, T. Kato, K. Nakai, S. Koseki, Y. Fujimura, Chem. Phys. 304 (2004) 203.
[17] Y. Sato, H. Kono, S. Koseki, Y. Fujimura, J. Am. Chem. Soc. 125 (2003) 8019.
[18] J.T. Paci, D.M. Wardlaw, J. Chem. Phys. 119 (2003) 7824.
[19] J.T. Paci, D.M. Wardlaw, A.D. Bandrauk, J. Phys. B 36 (2003) 3999.
[20] M.V. Korolkov, K.M. Weitzel, J. Chem. Phys. 123 (2005) 164308.
[21] T.D.G. Walsh, L. Strach, S.L. Chin, J. Phys. B 31 (1998) 4853.
[22] J.T. Paci, D.M. Wardlaw, J. Chem. Phys. 120 (2004) 1279.
[23] A. Conjusteau, A.D. Bandrauk, P.B. Corkum, J. Chem. Phys. 106 (1997) 9095.
[24] M. Thachuk, D.M. Wardlaw, J. Chem. Phys. 102 (1995) 7462.
[25] W.C. Swope, H.C. Andersen, P.H. Berens, K.R. Wilson, J. Chem. Phys. 76 (1982) 637.
[26] J. Zhou, H.B. Schlegel, J. Phys. Chem. A 115 (2011) 8375.
[27] M.J. Frisch et al., Gaussian Development Version Revision H.11, Gaussian Inc, Wallingford, CT, 2010.
[28] R. Mitric, J. Petersen, M. Wohlgemuth, U. Werner, V. Bonacic-Koutecky, Phys. Chem. Chem. Phys. 13 (2011) 8690.
[29] J.M. Millam, V. Bakken, W. Chen, W.L. Hase, H.B. Schlegel, J. Chem. Phys. 111 (1999) 3800.
[30] H. Wu, M. Rahman, J. Wang, U. Louderaj, W.L. Hase, Y. Zhuang, J. Chem. Phys. 133 (2010) 074101.
[31] M.V. Ammosov, N.B. Delone, V.P. Krainov, Sov. Phys. JETP 64 (1986) 1191.
[32] G.L. Yudin, M.Y. Ivanov, Phys. Rev. A 64 (2001) 013409.
[33] P.B. Corkum, Phys. Rev. Lett. 71 (1993) 1994.
[34] P. Dietrich, D.T. Strickland, M. Laberge, P.B. Corkum, Phys. Rev. A 47 (1993) 2305.